

Supplemental Material

I. Supplemental Methods:

Isolation of non-parenchymal fraction: Livers were perfused and digested using the pronase/collagenase method and cells were then centrifuged to pellet the hepatocytes. The remaining non-parenchymal cell fraction was in the supernatant (containing hepatic myofibroblasts (HSCs, portal fibroblasts and others), Kupffer cells (KC), BM cells and endothelial cells (EC)). aPFs and aHSCs were isolated using cell sorting for Col-GFP⁺Vit.A⁻ and Col-GFP⁺Vit.A⁺ cells. KC and EC were isolated by gradient centrifugation (15% Nycodenz) followed by magnetic sorting with anti-CD11b and anti-CD31 antibodies, respectively (Miltenyi Biotec). Cholangiocytes were a gift of Dr. Alpini, and were isolated from BDL mice.

Flow cytometry: Flow cytometry was based on simultaneous detection of collagen- α 1(I)-GFP (488 nm) and Vitamin A (autofluorescent signal detected by violet laser at 405 nm, Figure 2B) in Col-GFP mice. Phenotyping of the non-parenchymal fraction isolated from Col-GFP mouse livers was performed on a FACSCanto (BD). Cell sorting was performed on a MoFlo (Beckman Colter).

Immortalization of aPFs Isolated aPFs were incubated for 5 days on plastic dishes, and incubation with Lentivirus (GenTarget Inc, LVP016-puro) was started following the

manufacturer's instruction. The Lentivirus infected cells were selected by incubation with puromycin for 2 days.

Cell Culture and transfection Immortalized aPFs from wt mice and *Msln*^{-/-} mice were pre-treated with the following inhibitors: JAK inhibitor (AZD1480), MEK inhibitor (U0126), MEK1/2 inhibitor (PD98059), PI3 kinase inhibitor (iPI3K), mTOR inhibitor (Rapamycin,), JNK inhibitor (iJNK,), AKT inhibitor (iAKT), and JAK2 inhibitor (iJAK2) for 20min, and then incubated with either recombinant TGF- β 1(R&D, 240-B-002) or recombinant FGF(R&D, 3139-FB-025), the time points are indicated for each experiment. siRNAs against mouse Thy1 (Qiagen, FlexiTube GeneSolution GS21838 Cat No. 1027416) were transfected into *Msln*^{-/-} aPFs. Two siRNAs (# 1 and #4) suppressed the expression of the Thy1 protein (~80%) knockdown, compared to scrambled siRNA (Ctr). siRNAs were transfected according to the manufacturer's protocol. Briefly, siRNAs were applied to 1×10^5 of attached cells in a well of 6-well dish at 25nM final concentration, in culture medium with 7.5 μ l of RNA iMAX (Life Technologies). Cells were examined 24 hrs-6 days after transfection. The pAdEasy-based retroviral vector encoding *Msln* (Addgene, Plasmid #31305) was transfected into *Msln*^{+/+} and *Msln*^{-/-} aPFs. The adenovirus expressing constitutively active Akt encoding an amino-terminal myristylation signal (AdmyrAkt) and GFP expressing adenovirus (AdGFP) were described previously.

Western blotting The primary antibodies and dilutions were as follows: anti-*Msln* antibody (#28127; IBL) at 1:200; anti-Thy1 antibody (#9798; Cell Signaling Technology)

at 1:1000, anti-Muc16 antibody (#R2334-3; Abicode) at 1:500, pJak2 (#8082; Cell Signaling Technology) at 1:1000, Jak2 (#3230; Cell Signaling Technology) at 1:1000, β -actin at 1:5000, pStat3 (#9145; Cell Signaling Technology) at 1:2000; Stat3 (#9139; Cell Signaling Technology) at 1:2000, ERK1/2 (#9107; Cell Signaling Technology) at 1:2000, and pERK1/2 (#4370; Cell Signaling Technology) at 1:2000, pSmad2 (#3101; Cell Signaling Technology) at 1:1000, Smad2 (#5339; Cell Signaling Technology) at 1:1000, TGF β RI (#ab31013; Abcam) at 1:500, TGF β RII (#ab61213; Abcam) at 1:500, Smad7 (#sc-365846; Santa Cruz) at 1:200, pAKT (#9271; Cell Signaling Technology) at 1:1000, AKT (#sc-8312; Santa Cruz) at 1:1000, FGFR1 (#9740; Cell Signaling Technology) at 1:1000, pPI3K (#4228; Cell Signaling Technology) at 1:1000, PI3K (#4257; Cell Signaling Technology) at 1:1000, p-P38 (#9211; Cell Signaling Technology) at 1:1000, P38 (#sc-535; Santa Cruz) at 1:200, pJNK (#9251; Cell Signaling Technology) at 1:1000, JNK1/2 (#554285; BD Pharmingen) at 1:500.

Quantification of Immunofluorescence and immunohistochemistry: Images of seven non-overlapping fields were randomly selected and captured at $\times 100$ magnifications. Sirius red staining pictures were quantified by image analysis with National Institutes of Health image (Image J), using macros (<https://imagej.net/docs/examples/stained-sections/index.html>). Immunofluorescent sections were also quantified with image J macros with the same color threshold for each experiment. (<https://imagej.nih.gov/ij/developer/macro/macros.html>).

Immunoprecipitation To immunoprecipitate Msln, Mucin16 and TGF β R1 proteins, the cells were washed once with ice cold PBS and lysed in a lysis buffer containing 50 mM Tris-HCl (pH 7.4), 300 mM NaCl, 10mM HEPES, 0.5% NP-40, 2.5mM CHAPS, 10 mM NaF, 1 mM Na₃VO₄, 5% Glycerol, 25mM EDTA, 2mM EGTA, 1mM Sodium Deoxylate, and a protease inhibitor cocktail . The whole cell lysates were pre-cleared with rProtein G Sepharose Fast Flow (GE Healthcare, Chalfont St Giles, England) at 4°C for 1 h. The cell lysates were then incubated at 4°C overnight with 2ug of anti-Msln antibody (#28127; IBL), anti-TGF β R1 (#ab31013; Abcam) antibody or anti-Muc16 (#R2334-3; Abicodex) antibody. The immune complexes were collected after incubation for 4 h at 4°C with protein G Sepharose (GE Healthcare). After washing three times in a wash buffer, the immunoprecipitates were boiled in 2X sample buffer for 10 min and subjected to western blotting.

Immunocytochemistry Primary wt and Msln^{-/-} aPFs were stimulated with recombinant FGF(2 ng/ml, R&D), and stained with anti-Ki67 Ab (GeneTex gtx16667) or isotype control followed by secondary Alexa Fluor 594 antibodies. Collagen-GFP expression was visualized by fluorescent microscopy.

II. Supplemental Figures:

Suppl. Figure 1. DDC- and BDL-induced cholestatic fibrosis is attenuated in Msln^{-/-} mice.

A. DDC-injured Msln^{-/-} mice developed less liver fibrosis than wt mice. Msln^{-/-} mice and wt littermates (n=7/group) were fed with DDC or control diet (3 weeks), were stained

with Sirius Red, and positive area was quantified as percent using Image J. Liver function was assessed by serum levels ALT and ALP (IU/L). Expression of fibrogenic (Coll1a1, α -SMA, TGF- β 1), inflammatory (F4/80), and aPF-specific (Msln and Fibulin2) gene mRNA was determined by qPCR of total liver tissue, the data are fold induction (vs sham wt mice). P values were determined using 2-tailed Student's t test * $p < 0.05$, ** $p < 0.01$ (supports Figure 1). B-C Msln^{-/-}Col-GFP and wt Col-GFP littermates (n > 8 per group) were (B) sham- or (C) BDL- (5 days) operated, livers were co-stained for DAPI, Thy-1 and Desmin. Positive area of GFP⁺Thy-1⁺ staining was calculated using Image J. Representative images (taken using objective x 20) are shown. The same representative images for the WT and Msln^{-/-} Thy-1/Dapi panels, and Col-GFP/DAPI panels are also shown in Figure 2A. Anti-Msln Ab was not used for immunohistochemistry due to the non-specific crossreactivity to the mesothelin-like protein. D BDL- (5 days)-operated Col-GFP (wt) and Msln^{-/-}Col-GFP mice (ko) (n > 8 per group). Livers were co-stained with DAPI, Thy-1, Desmin, the area of overlapping Thy-1⁺ or Desmin⁺ staining is shown. Although Thy-1⁺ aPFs and Desmin⁺ aHSCs are located in the fibrotic areas, there is little overlap between Thy-1 and Desmin staining (supports Figure 2) .

Suppl. Figure 2. GPM6A⁺ mesothelial cells minimally contribute to cholestatic fibrosis in BDL-operated wt Col-GFP mice.

A-B. Wt Col-GFP mice (n > 8 per group) were sham- or BDL- (5 days) operated, livers were co-stained for GPM6A, DAPI, or Thy-1. **A.** Expression of GPM6A was observed only in GFP⁺ myofibroblasts located within the liver capsule (LC), representative images

were taken using x 40 objective. **B.** Expression of Col-GFP was not observed in cholangiocytes of BDL (5 days)-injured Col-GFP mice. BD – bile duct. **C.** Wt and Thy-1^{-/-} mice livers were BDL- (5 days) operated, livers were stained for Thy-1. The specificity of the anti-Thy-1 Ab was tested. Expression of Thy-1 was strongly upregulated in livers the of the wt BDL-mice (portal areas) vs sham-wt mice (in which Thy-1 staining was mostly observed in T cells). Immunostaining with anti-Thy-1 Ab was not observed in sham- or BDL-Thy-1^{-/-} mice. Representative images, (objectives x 4, x 10, x 20), BD-bile ducts, V- portal vein, LP- liver parenchyma. **D.** Expression of Msln and Thy-1 was compared by qRT-PCR in purified endothelial cells (EC), Kupffer cells (KC), BDL-activated HSCs (aHSCs) and aPFs, sham- and BDL-activated cholangiocytes (gift of Dr. Alpini), and hepatic mesothelial cells isolated from the liver capsule of BDL-operated Col-GFP mice. The purity of each cellular fraction was estimated by qRT-PCR for expression of F4/80 in KC, CD31 in EC, Lrat, GFAP and Desmin in HSCs, Thy1 in aPFs, and K19 in cholangiocytes (not shown). The data (from three independent experiments) are shown as relative mRNA expression (supports Figure 2).

Suppl. Figure 3. BDL (5 days) fibrosis was attenuated in Msln-ablated Msln^{DTA} mice by ≈50% compared to wt Msln^{nLacZ} mice.

A. Tamoxifen administration (12 x 5 mg/mouse/oral gavage, prior to BDL) irreversibly labeled all Msln⁺ aPFs by nuclear LacZ (nLacZ) expression in wt Msln^{nLacZ} mice, and caused ablation of nLacZ⁺ aPFs in Msln^{DTA} littermates. Livers were stained for LacZ, and sectioned. The sagittal cut across the liver parenchyma is shown. LacZ⁺ cells are equally distributed throughout the liver parenchyma. Micrographs are gross livers, images are

taken using objective x 40. B. Liver sections were immunostained and analyzed for the overlapping expression of Thy-1⁺ and α -SMA⁺ in DAPI⁺ cells, representative images are shown (objective x 20). The same representative images for merged Msln(nLacZ) and Msln(DTA) are shown in Figure 3C. C. The number of F4/80⁺ Kupffer cells was not significantly changed in BDL (5 days)-injured livers of Msln^{nLacZ} and Msln^{DTA} mice. Livers of wt Msln^{nLacZ} and Msln^{DTA} mice were stained with anti-F4/80 antibody. Micrographs are representative images. Positive area was quantified by Image J, and shown as percent. P values were determined using ANOVA, *p<0.05, non-specific (supports Figure 3).

Suppl. Figure 4. Thy-1⁺Msln⁺ α -SMA⁺ aPFs were detected in livers of patients with cholestatic liver injury.

Liver serial sections from patients with biliary atresia (n=6), secondary biliary fibrosis (Metavir Score: F2, n=5), and HCV fibrosis (F2, n=5), or normal livers (n=4) were stained for collagen deposition (Sirius Red), α -SMA (activated myofibroblasts), Thy1 and Msln (markers of activated aPFs), and Desmin (HSC marker). Micrographs are serial sections; images are taken using objective x 10 (supports Figure 4).

Suppl. Figure 5. Characterization of isolated primary aHSCs and aPFs

Primary GFP⁺VitaminA⁻ aPFs were sort purified from livers of BDL (5 d) wt and Msln^{-/-} mice, and analyzed using qPCR for mRNA expression of lineage-specific signature genes,

characteristic for HSCs (p75, Synemin, Lrat, Desmin, GFAP, etc) and aPFs (elastin, Thy-1, fibulin 2 (fib2), supports Figure 5).

Suppl. Figure 6. Immunoprecipitations (IP) from cell lysates of wt or *Msln*^{-/-} aPFs ± TGF-β1.

A. IP with anti-TGFβRI Ab: To gain insight into the amount of *Msln*, *Muc16*, and *Thy1*, and *Smad7* protein within the complex pulled down using TGFβRI, the amount of immunoprecipitated TGFβRI was normalized. The levels of precipitated TGFβRI was detected using immunoblotting with anti-TGFβRI Ab, and demonstrate that similar amount of TGFβRI was used for the Western blotting analysis in Figure 5C. **B.** IP with anti-*Msln* Ab: the levels of precipitated *Msln* was detected using immunoblotting with anti-*Msln* Ab, suggesting that similar amount of *Msln* was used for Western blotting in Figure 5D. **C.** IP with anti-*Muc16* Ab: the levels of precipitated *Muc16* was detected using immunoblotting with anti-*Muc16* Ab, suggesting that similar amount of *Muc16* was used for Western blotting in Figure 5E. Images representative of > three independent IPs are shown (supports Figure 6).

Suppl. Figure 7. *Msln*-*Muc16* signaling regulates activation of aPF/myofibroblasts in BDL-injured mice.

Liver fibrosis was compared in BDL (5 d)-operated *Msln*^{-/-}, *Muc16*^{-/-} and *Msln*^{-/-}*Muc16*^{-/-} and wt littermates (n = 8 per group, see Figure 7). Livers were immunostained for α-SMA, positive area was quantified. Micrographs are Sirius Red staining (x 4 objective),

the data are percent of positive area. P values were analyzed using ANOVA, *p<0.05, ns - non-specific.

Suppl. Figure 8. Regulation of FGF signaling pathways in wt aPFs.

Immortalized wt aPFs (10^5 /well) were pretreated for 20 min with DMSO or inhibitors: i-FGFR; i-JAK2+ERK1/2 (AZD1480, 1 μ M), i-MEK (PD98059, 10 μ M), i-MEK (U0126, 5 μ M), i-TGF β RI (LY364947, 1 μ M), i-TGF β RI/II (LY2109761, 10 μ M), i-PI3K (Wortmannin, 0.5 μ M), i-mTOR (Rapamycin, 2 μ g/ml) i-JNK (SP600125, 20 μ M), i-AKT (Akt Inhibitor IV, 0.5 μ M), and i-JAK2 (TG-101348, 1 μ M), and stimulated \pm FGF (2 ng/ml, 6h). Cyclin D mRNA was measured, the data are fold induction (vs untreated aPFs), the average of > three independent experiments (supports Figure 10).

Suppl. Figure 9. Reconstitution of Msln in Msln^{ko+Msln} aPFs.

A. Msln cDNA was cloned into pCMV-Tag3A expression vector (which also contains *myc* tag at N-terminus, pCMV-Myc) to generate pCMV-Msln-Myc vector. Wt and Msln^{-/-} (Msln^{ko+Msln}) aPFs were transfected either with control vector pCMV-Myc, or pCMV-Msln-Myc. Transfection efficiency was estimated in wt and Msln^{-/-} aPFs by expression of Myc protein using immunostaining with anti-Myc Ab. Similar levels of Myc expression were observed in all transfected cells. Representative images are shown (using objective x 60). **B.** Wt, Msln^{ko+Msln} and Msln^{-/-} aPFs were re-plated after 72 h post transfection (10^4 /well), allowed to adhere overnight (18 h), and analyzed by scratch assay (12 h). The images are bright field (BF) and fluorescent (Col-GFP, taken using objective x 4, average of > three experiments). **C.** Expression of Cyclin D was restored in FGF (2 ng/ml, 6h)-

stimulated $Msln^{ko+Msln}$ aPFs and blocked in the presence of AZD1480, P values were determined using ANOVA, * $p < 0.05$, ns - non-specific, (supports Figure 11).

Suppl. Figure 10. Blocking of Thy-1 does not affect expression levels of ERK1/2 in $Msln^{ko-siThy-1}$ aPFs.

$Msln^{-/-}$ aPFs were transfected with control (Ctrl) or Thy-1 (#1, and #4) siRNAs. Expression and phosphorylation of ERK1/2 was evaluated by immunoblotting, normalized to β -actin protein expression level (supports Figure 12).

Suppl. Figure 11. Reconstitution of AKT restores proliferation and migration of $Msln^{-/-}$ aPFs.

A. $Msln^{-/-}$ aPFs were infected with constitutively active (CA) AKT ($Msln^{ko-AAV-CA-AKT}$ aPFs). Phosphorylation of JAK2 was restored in $Msln^{ko-AAV-CA-AKT}$ aPFs, normalized to JAK2 protein expression level. **B.** Expression and phosphorylation of ERK1/2 was detected by immunoblotting, normalized to β -actin protein expression level. **C.** TGF- β 1-induced phosphorylation of Smad2 was not restored in $Msln^{ko-AAV-CA-AKT}$ aPFs (supports Figure 13).

Supplemental Figure 1

A

Diet, 3 weeks

Control

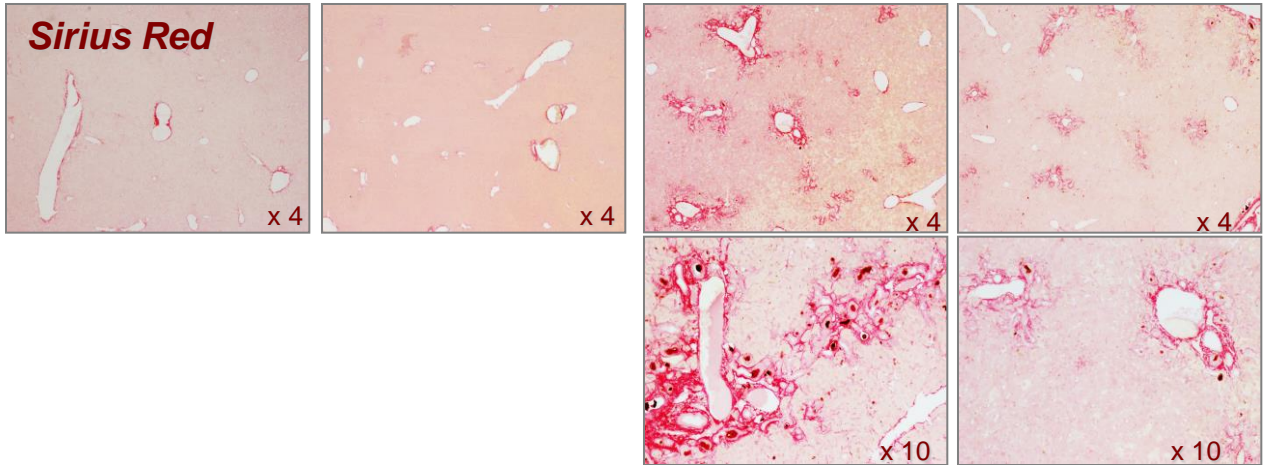
DDC

Wt

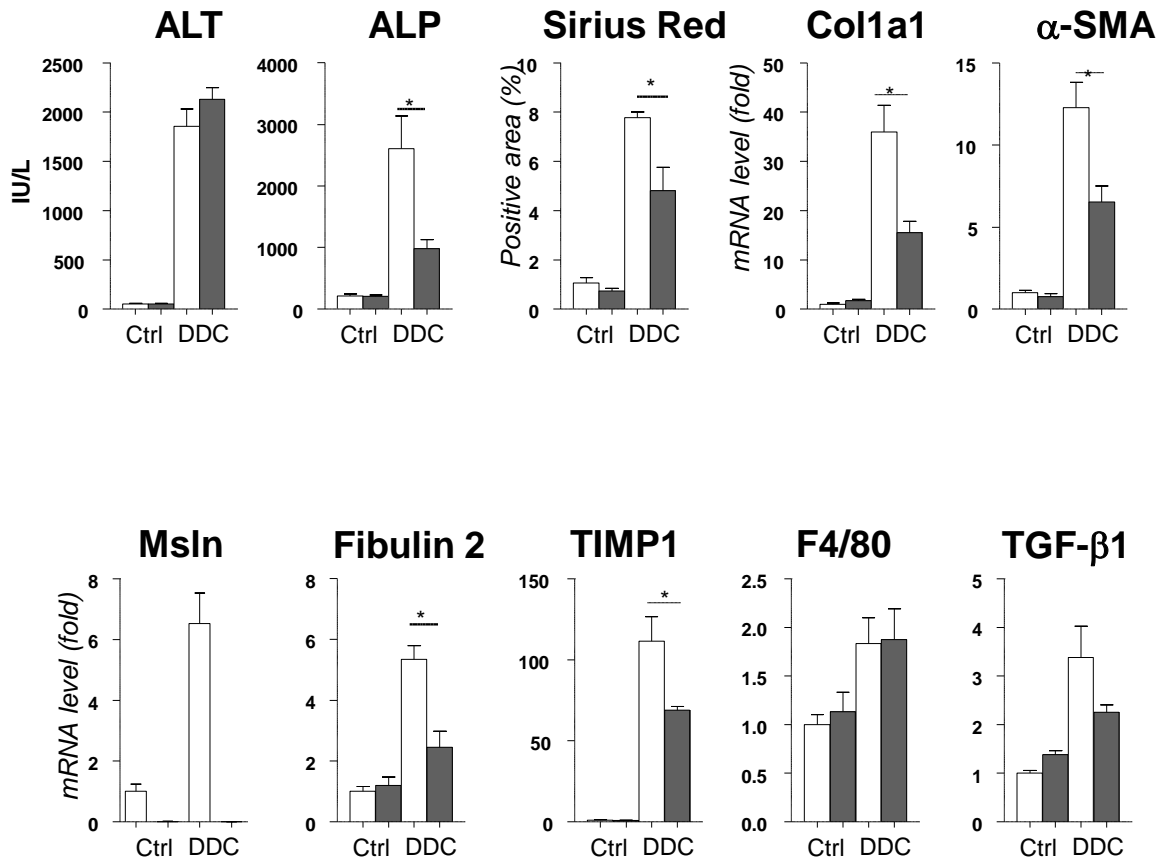
Msln^{-/-}

Wt

Msln^{-/-}

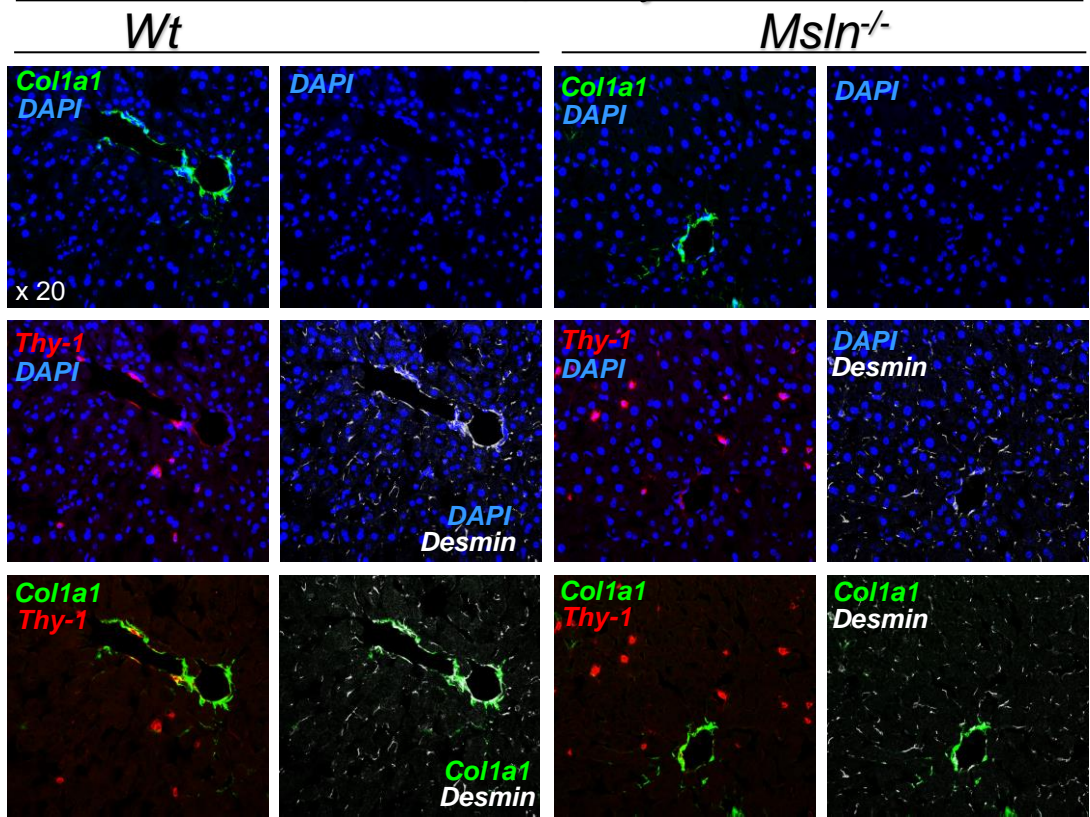


□ *Wt* mice ■ *Msln*^{-/-} mice

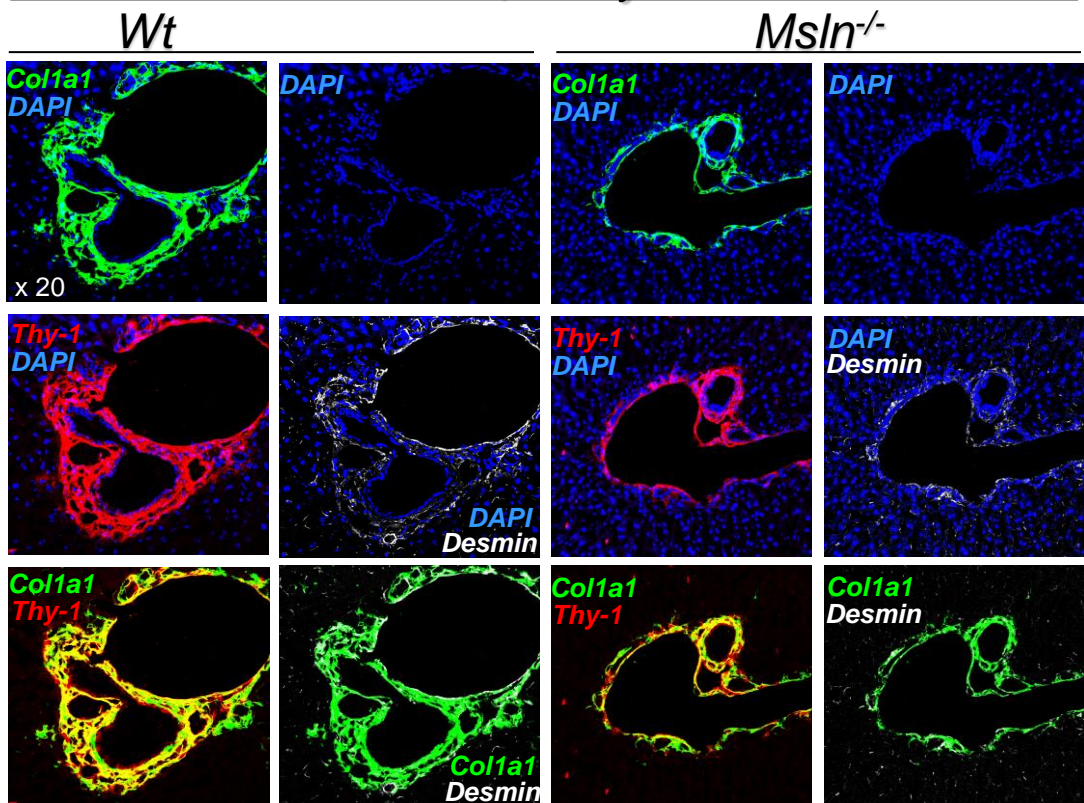


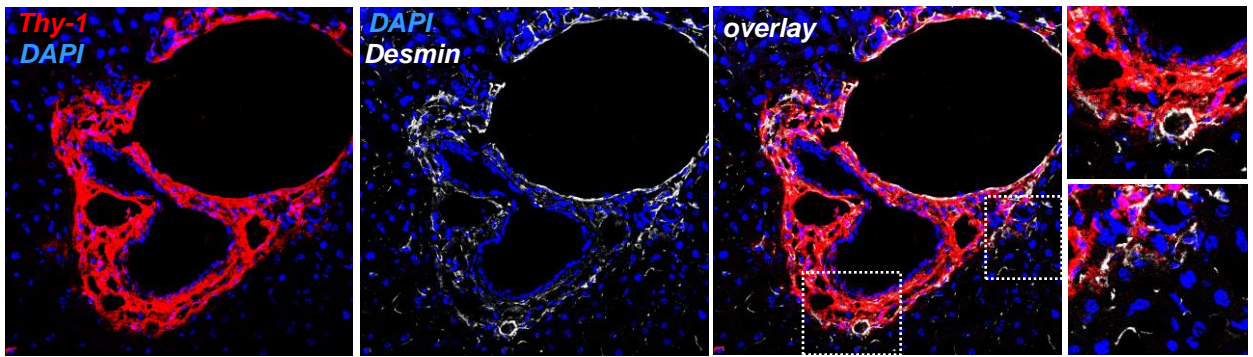
B

Sham, 5 days

**C**

BDL, 5 days

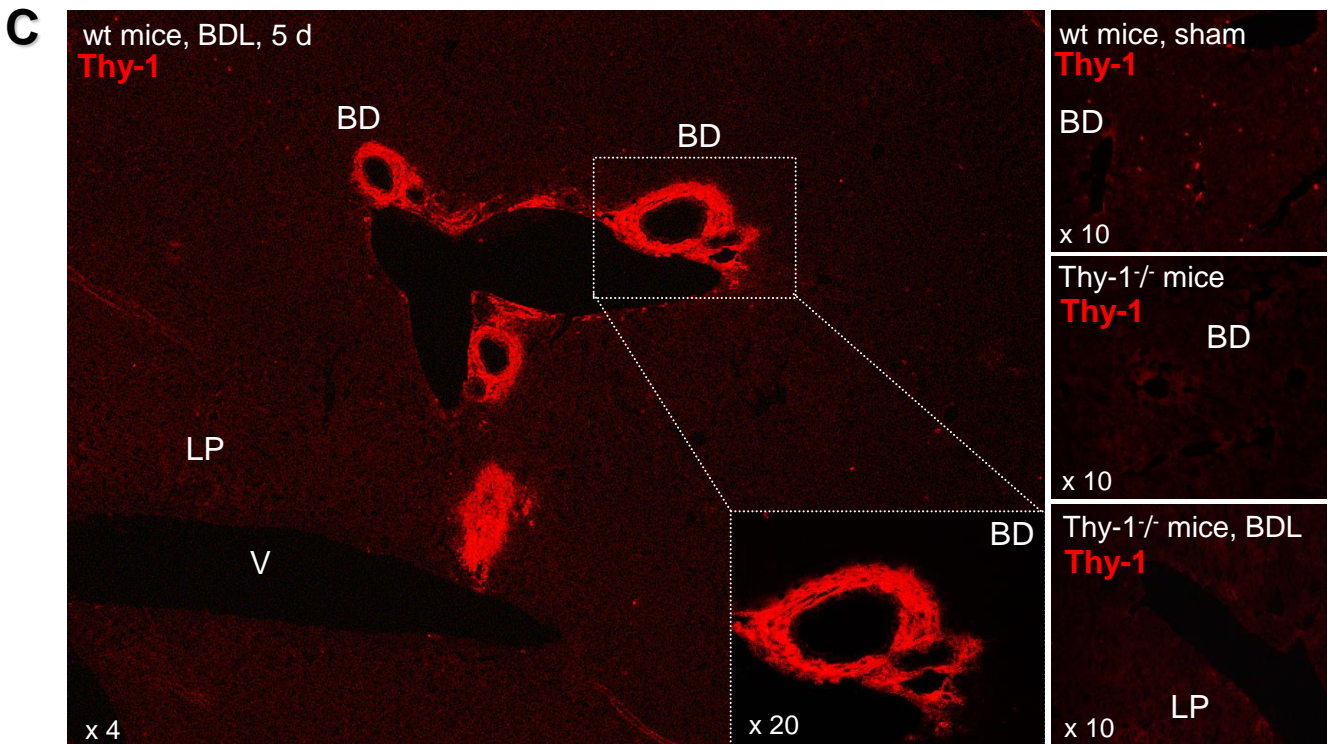
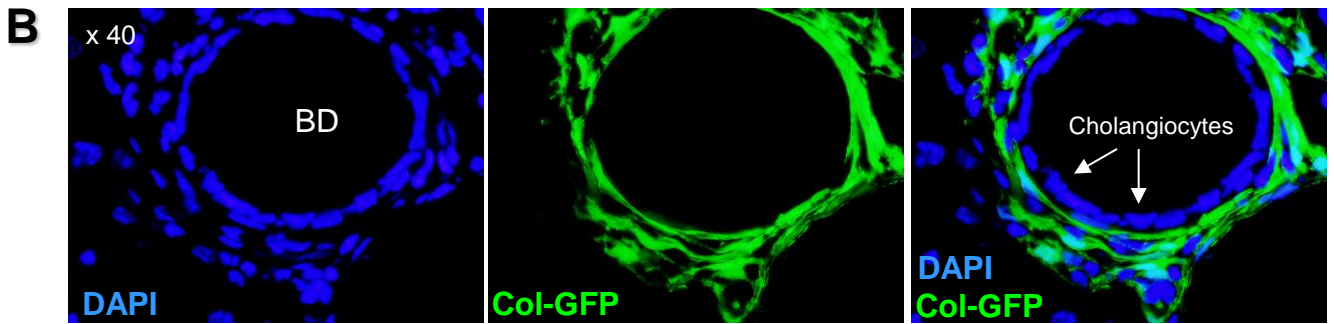
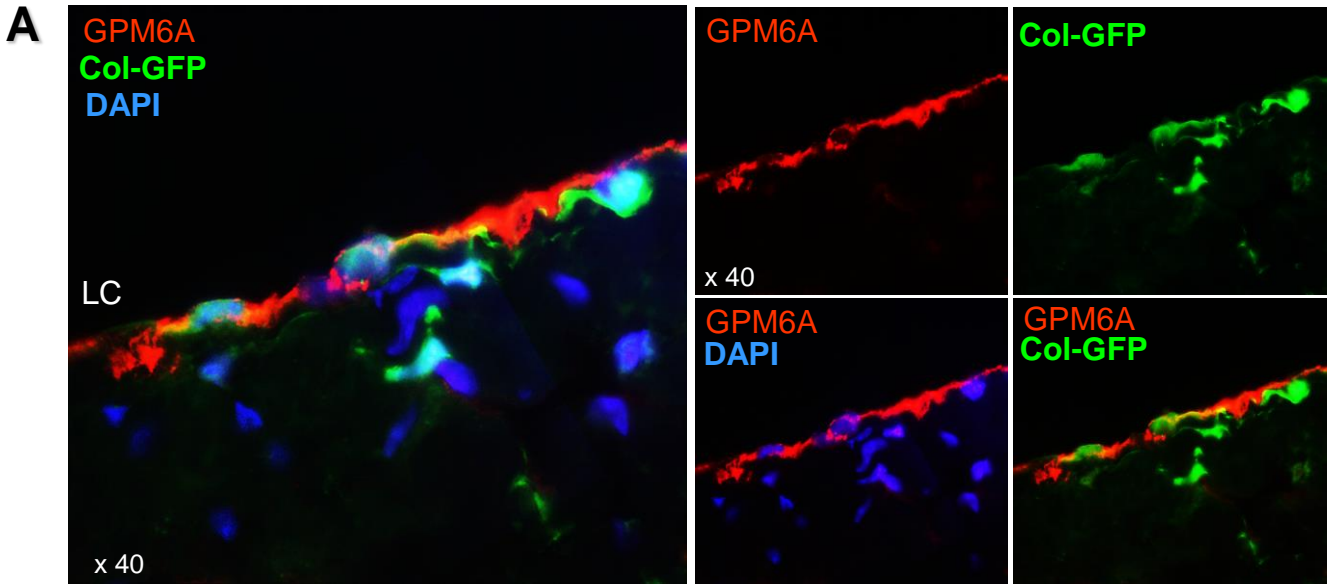


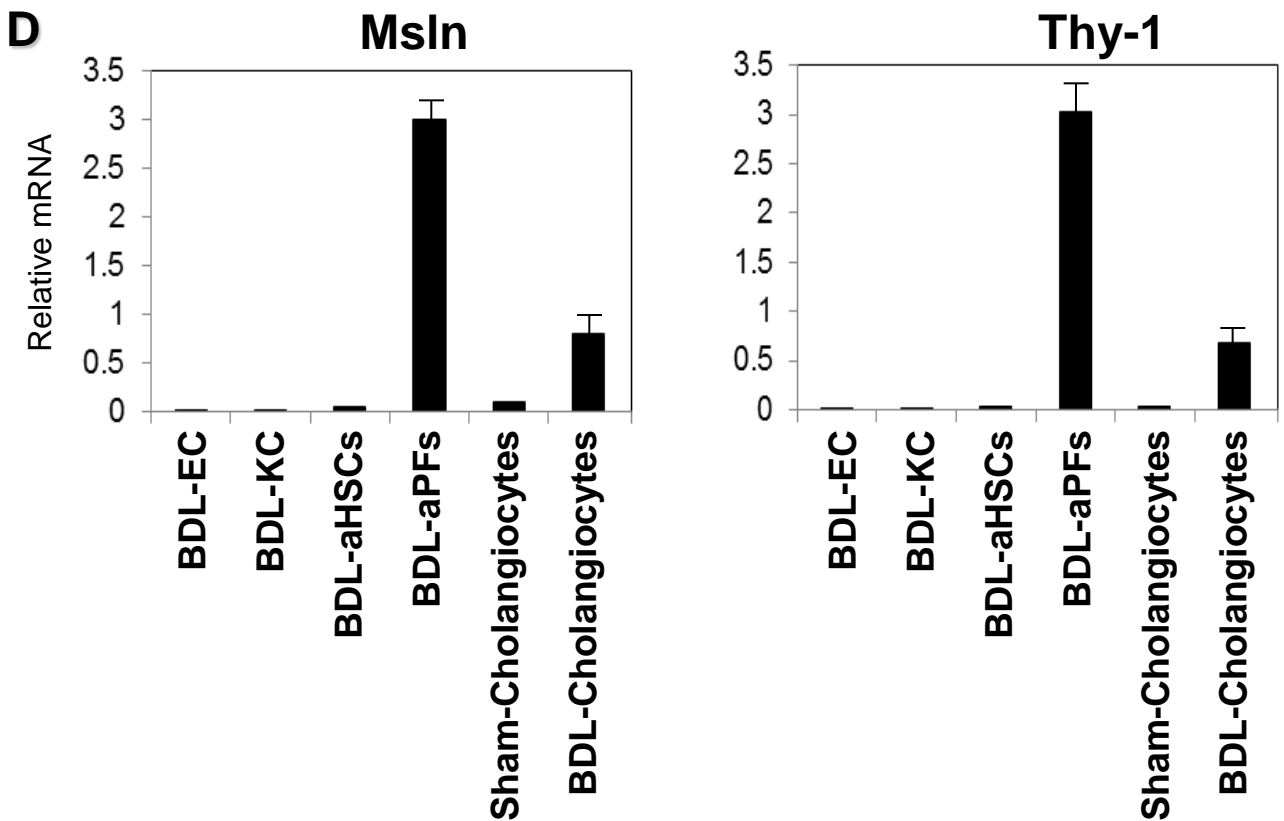
D

Suppl. Figure 1. DDC- and BDL-induced cholestatic fibrosis is attenuated in *Msln*^{-/-} mice.

A. DDC-injured *Msln*^{-/-} mice developed less liver fibrosis than wt mice. *Msln*^{-/-} mice and wt littermates (n=7/group) were fed with DDC or control diet (3 weeks), were stained with Sirius Red, and positive area was quantified as percent using Image J. Liver function was assessed by serum levels ALT and ALP (IU/L). Expression of fibrogenic (Col1a1, α -SMA, TGF- β 1), inflammatory (F4/80), and aPF-specific (*Msln* and *Fibulin2*) gene mRNA was determined by qPCR of total liver tissue, the data are fold induction (vs sham wt mice). P values were determined using 2-tailed Student's t test *p<0.05, **p<0.01 (supports Figure 1). **B-C** *Msln*^{-/-}Col-GFP and wt Col-GFP littermates (n > 8 per group) were (**B**) sham- or (**C**) BDL- (5 days) operated, livers were co-stained for DAPI, Thy-1 and Desmin. Positive area of GFP⁺Thy-1⁺ staining was calculated using Image J. Representative images (taken using objective x 20) are shown. The same representative images for the WT and *Msln*^{-/-} Thy-1/Dapi panels, and Col-GFP/DAPI panels are also shown in Figure 2A. Anti-*Msln* Ab was not used for immunohistochemistry due to the non-specific crossreactivity to the mesothelin-like protein. **D** BDL- (5 days)-operated Col-GFP (wt) and *Msln*^{-/-}Col-GFP mice (ko) (n > 8 per group). Livers were co-stained with DAPI, Thy-1, Desmin, the area of overlapping Thy-1⁺ or Desmin⁺ staining is shown. Although Thy-1⁺ aPFs and Desmin⁺ aHSCs are located in the fibrotic areas, there is little overlap between Thy-1 and Desmin staining (supports Figure 2) .

Supplemental Figure 2

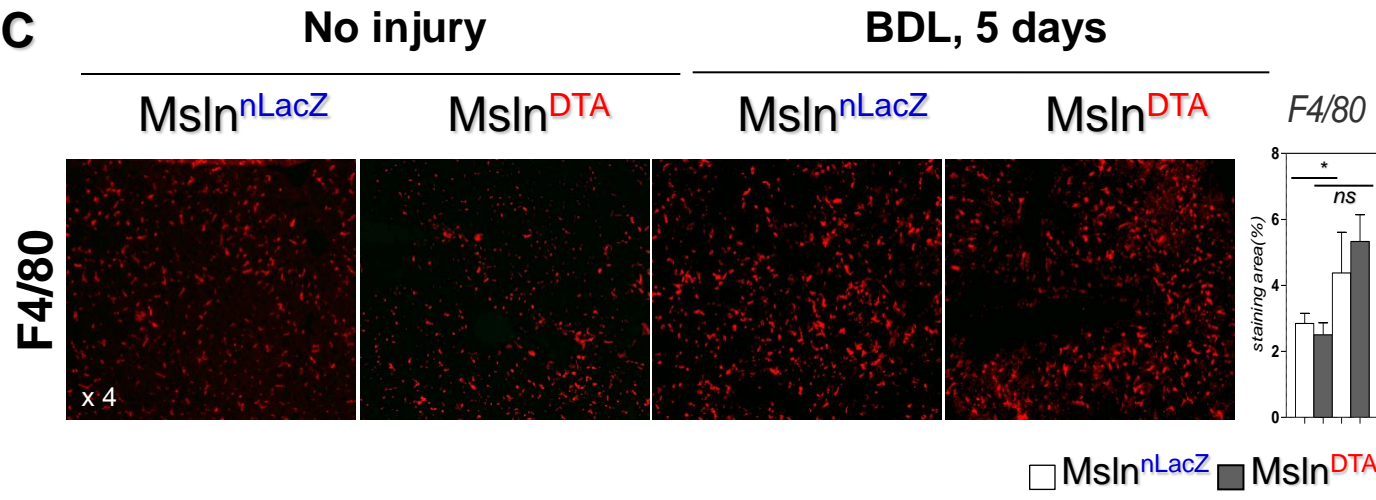
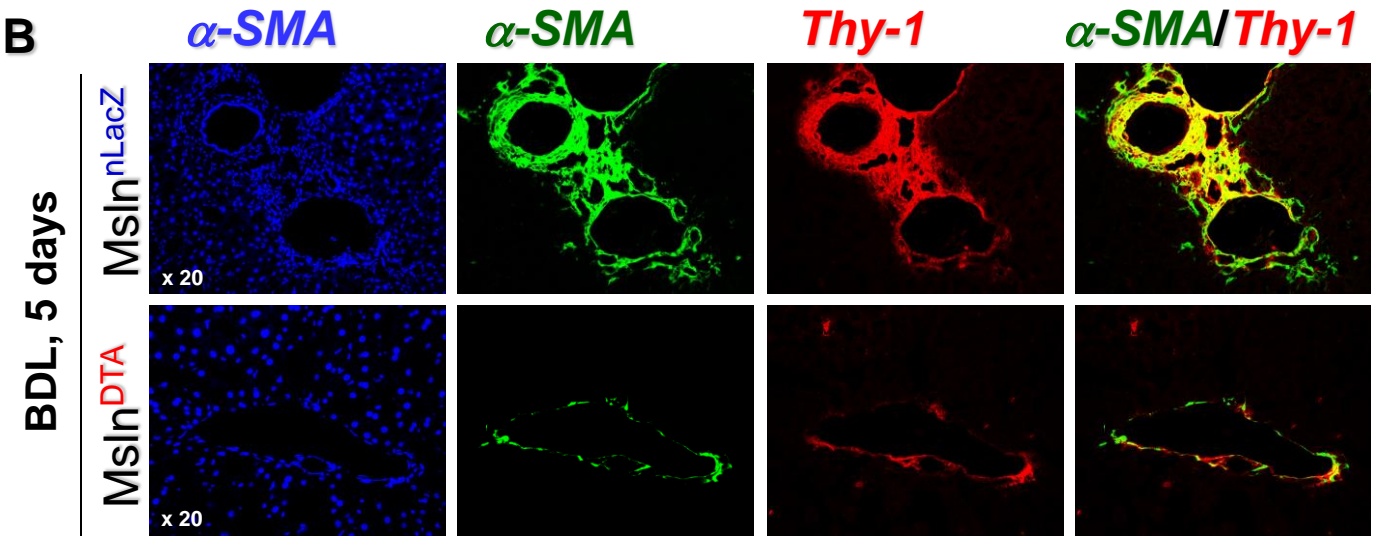
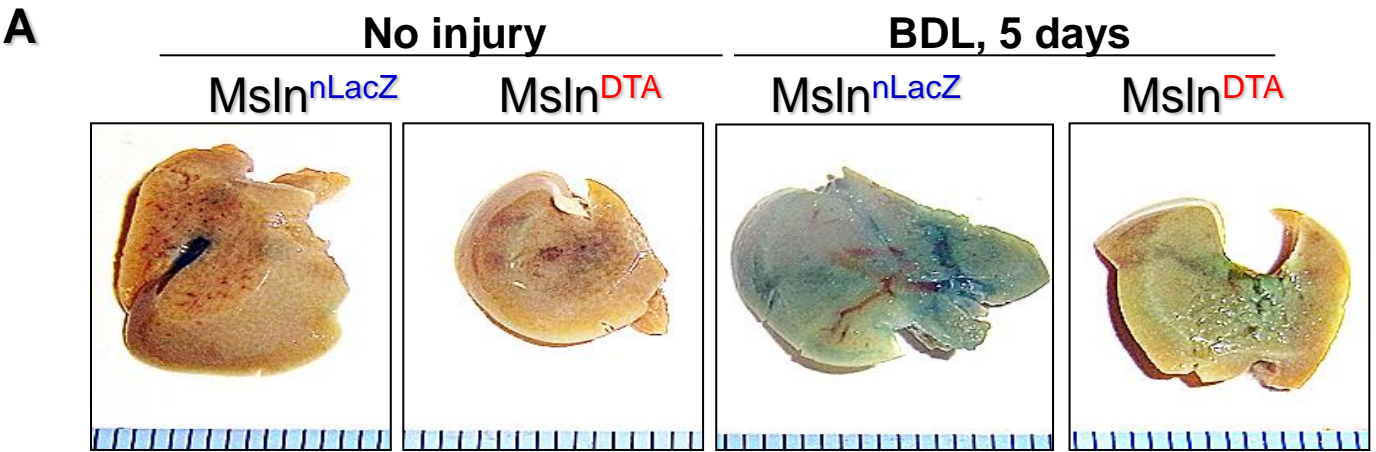




Suppl. Figure 2. GPM6A⁺ mesothelial cells minimally contribute to cholestatic fibrosis in BDL-operated wt Col-GFP mice.

A-B. Wt Col-GFP mice ($n > 8$ per group) were sham- or BDL- (5 days) operated, livers were co-stained for GPM6A, DAPI, or Thy-1. **A.** Expression of GPM6A was observed only in GFP⁺ myofibroblasts located within the liver capsule (LC), representative images were taken using x 40 objective. **B.** Expression of Col-GFP was not observed in cholangiocytes of BDL (5 days)-injured Col-GFP mice. BD – bile duct. **C.** Wt and Thy-1^{-/-} mice livers were BDL- (5 days) operated, livers were stained for Thy-1. The specificity of the anti-Thy-1 Ab was tested. Expression of Thy-1 was strongly upregulated in livers the of the wt BDL-mice (portal areas) vs sham-wt mice (in which Thy-1 staining was mostly observed in T cells). Immunostaining with anti-Thy-1 Ab was not observed in sham- or BDL-Thy-1^{-/-} mice. Representative images, (objectives x 4, x 10, x 20), BD-bile ducts, V- portal vein, LP- liver parenchyma. **D.** Expression of Msln and Thy-1 was compared by qRT-PCR in purified endothelial cells (EC), Kupffer cells (KC), BDL-activated HSCs (aHSCs) and aPFs, sham- and BDL-activated cholangiocytes (gift of Dr. Alpini), and hepatic mesothelial cells isolated from the liver capsule of BDL-operated Col-GFP mice. The purity of each cellular fraction was estimated by qRT-PCR for expression of F4/80 in KC, CD31 in EC, Lrat, GFAP and Desmin in HSCs, Thy1 in aPFs, and K19 in cholangiocytes (not shown). The data (from three independent experiments) are shown as relative mRNA expression (supports Figure 2).

Supplemental Figure 3

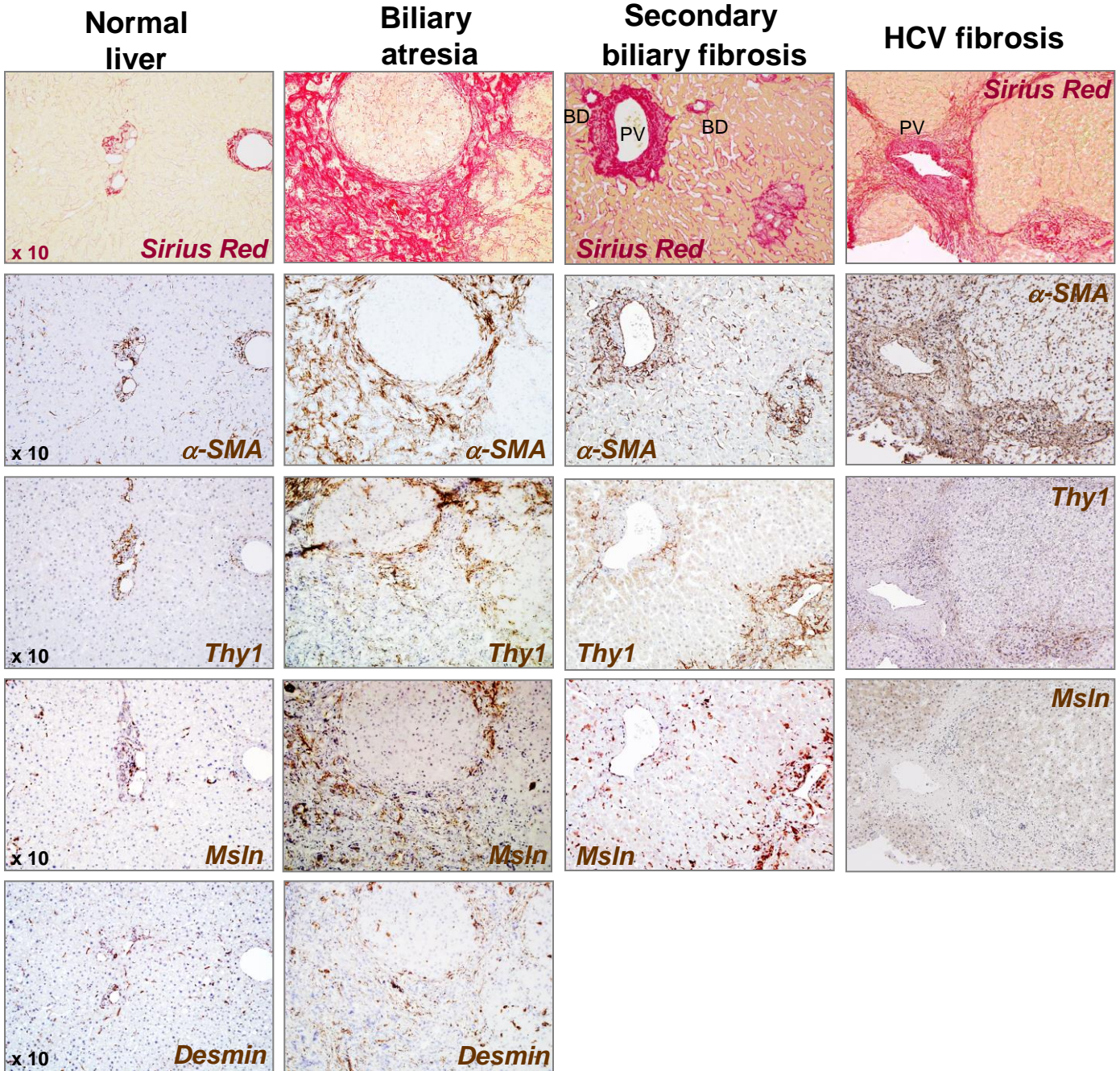


Suppl. Figure 3. BDL (5 days) fibrosis was attenuated in Msln-ablated Msln^{DTA} mice by ≈50% compared to wt Msln^{nLacZ} mice.

A. Tamoxifen administration (12 x 5 mg/mouse/oral gavage, prior to BDL) irreversibly labeled all Msln⁺ aPFs by nuclear LacZ (nLacZ) expression in wt Msln^{nLacZ} mice, and caused ablation of nLacZ⁺ aPFs in Msln^{DTA} littermates. Livers were stained for LacZ, and sectioned. The sagittal cut across the liver parenchyma is shown. LacZ⁺ cells are equally distributed throughout the liver parenchyma. Micrographs are gross livers, images are taken using objective x 40. **B.** Liver sections were immunostained and analyzed for the overlapping expression of Thy-1⁺ and α -SMA⁺ in DAPI⁺ cells, representative images are shown (objective x 20). The same representative images for merged Msln(nLacZ) and Msln(DTA) are shown in Figure 3C. **C.** The number of F4/80⁺ Kupffer cells was not significantly changed in BDL (5 days)-injured livers of Msln^{nLacZ} and Msln^{DTA} mice. Livers of wt Msln^{nLacZ} and Msln^{DTA} mice were stained with anti-F4/80 antibody. Micrographs are representative images. Positive area was quantified by Image J, and shown as percent. P values were determined using ANOVA, *p<0.05, non-specific (supports Figure 3).

Supplemental Figure 4

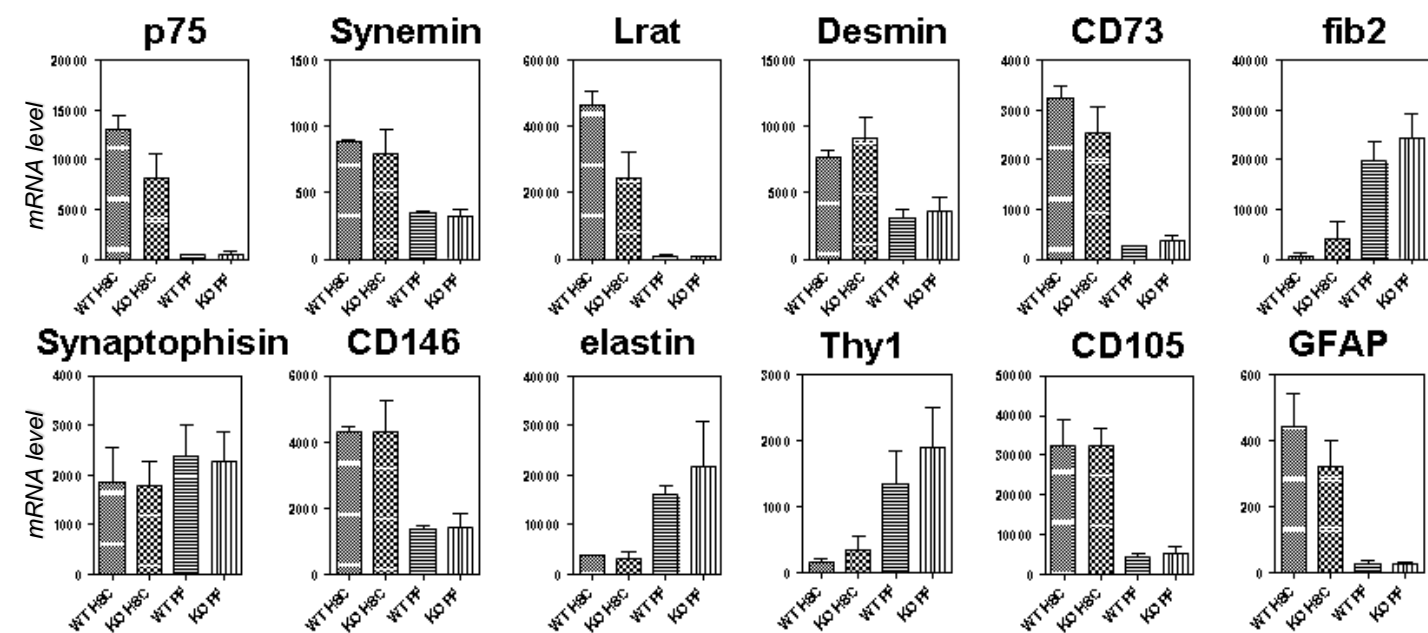
Patient material



Suppl. Figure 4. Thy-1⁺Msln⁺α-SMA⁺ aPFs were detected in livers of patients with cholestatic liver injury.

Liver serial sections from patients with biliary atresia (n=6), secondary biliary fibrosis (Metavir Score: F2, n=5), and HCV fibrosis (F2, n=5), or normal livers (n=4) were stained for collagen deposition (Sirius Red), α-SMA (activated myofibroblasts), Thy1 and Msln (markers of activated aPFs), and Desmin (HSC marker). Micrographs are serial sections, the images are taken using objective x 10 (supports Figure 4).

Supplemental Figure 5

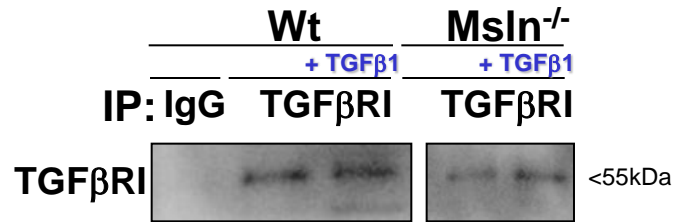


Suppl. Figure 5. Characterization of isolated primary aHSCs and aPFs.

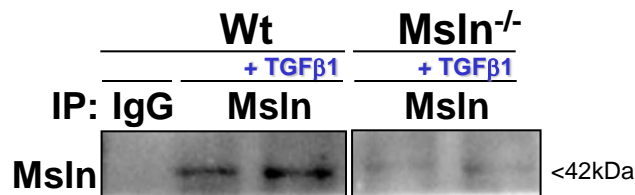
Primary GFP⁺VitaminA⁻ aPFs were sort purified from livers of BDL (5 d) wt and *Msln*^{-/-} mice, and analyzed using qPCR for mRNA expression of lineage-specific signature genes, characteristic for HSCs (p75, Synemin, Lrat, Desmin, GFAP, etc) and aPFs (elastin, Thy-1, fibulin 2 (fib2), supports Figure 5).

Supplemental Figure 6

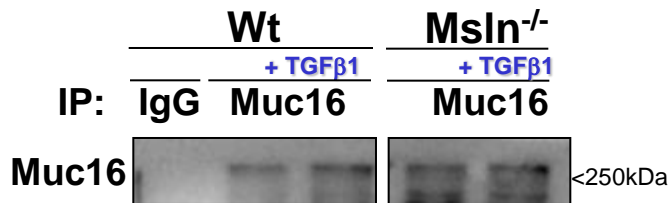
A



B



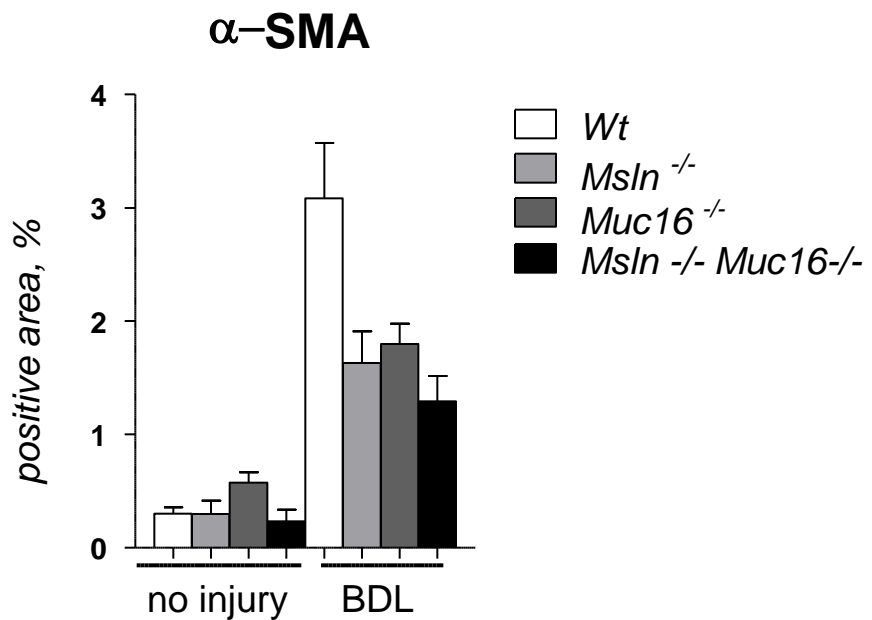
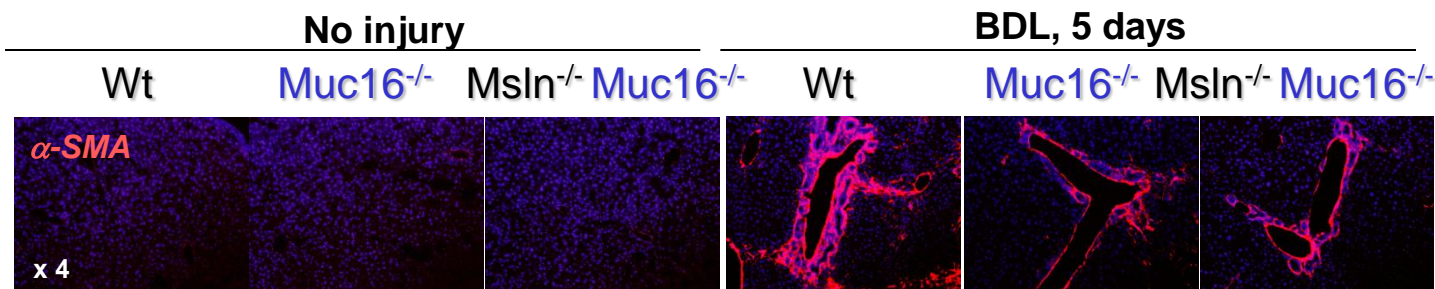
C



Suppl. Figure 6. Immunoprecipitations (IP) from cell lysates of wt or Msln^{-/-} aPFs ± TGF-β1. **A.** IP with anti-TGFβRI Ab: To gain insight into the amount of Msln, Myc16, and Thy1, and Smad7 protein within the complex pulled down using TGFβRI, the amount of immunoprecipitated TGFβRI was normalized. The levels of precipitated TGFβRI was detected using immunoblotting with anti-TGFβRI Ab, and demonstrate that similar amount of TGFβRI was used for the Western blotting analysis in Figure 5C. **B.** IP with anti-Msln Ab: the levels of precipitated Msln was detected using immunoblotting with anti-Msln Ab, suggesting that similar amount of Msln was used for Western blotting in Figure 5D. **C.** IP with anti-Muc16 Ab: the levels of precipitated Muc16 was detected using immunoblotting with anti-Muc16 Ab, suggesting that similar amount of Muc16 was used for Western blotting in Figure 5E. Images representative of > three independent IPs are shown (supports Figure 6).

Supplemental Figure 7

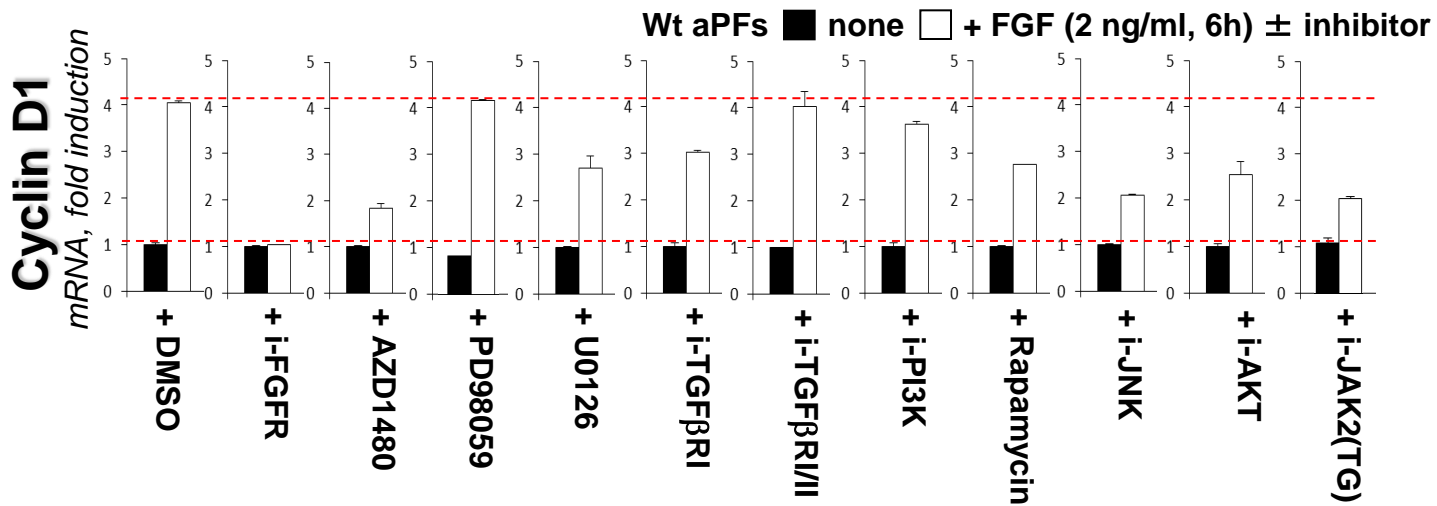
Msln^{-/-} mice, *Muc16*^{-/-} mice vs *Msln*^{-/-}*Muc16*^{-/-} mice



Suppl. Figure 7. *Msln*-*Muc16* signaling regulates activation of aPF/myofibroblasts in BDL-injured mice.

Liver fibrosis was compared in BDL (5 d)-operated *Msln*^{-/-}, *Muc16*^{-/-} and *Msln*^{-/-}*Muc16*^{-/-} and wt littermates (n = 8 per group, see Figure 7). Livers were immunostained for α -SMA, positive area was quantified. Micrographs are Sirius Red staining (x 4 objective), the data are percent of positive area. P values were analyzed using ANOVA, ns - non-specific.

Supplemental Figure 8

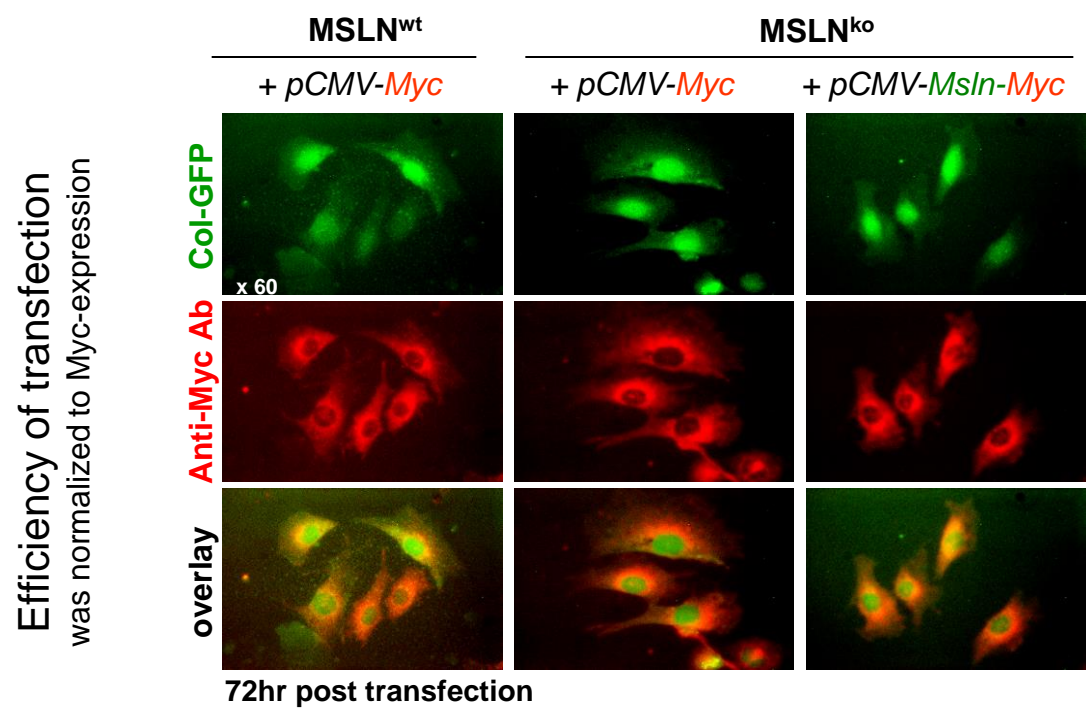


Suppl. Figure 8. Regulation of FGF signaling pathways in wt aPFs.

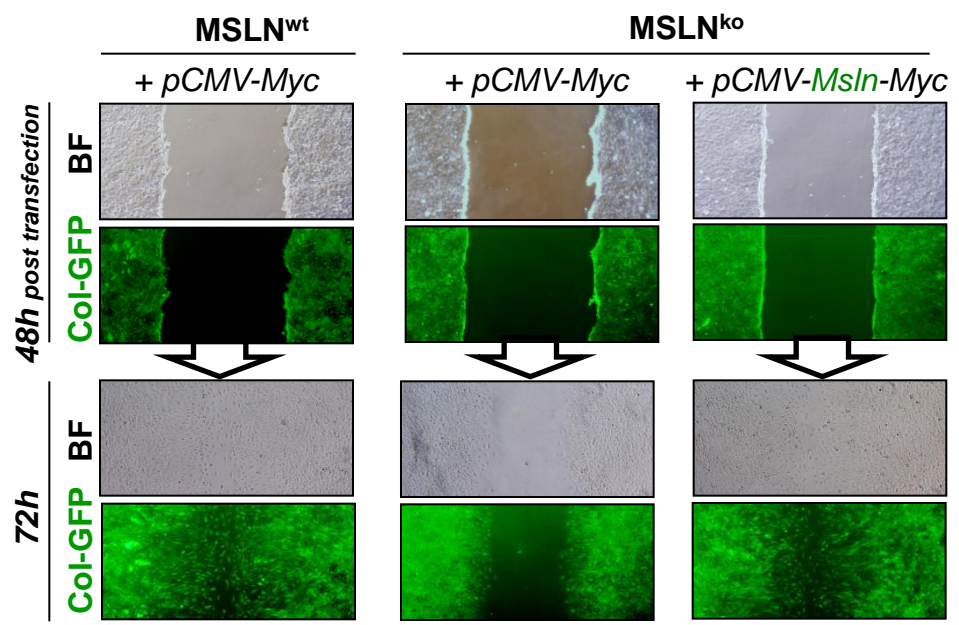
A. Immortalized wt aPFs (10^5 /well) were pretreated for 20 min with DMSO or inhibitors: i-FGFR; i-JAK2+ERK1/2 (AZD1480, $1\mu\text{M}$), i-MEK (PD98059, $10\mu\text{M}$), i-MEK (U0126, $5\mu\text{M}$), i-TGFβRI (LY364947, $1\mu\text{M}$), i-TGFβRI/II (LY2109761, $10\mu\text{M}$), i-PI3K (Wortmannin, $0.5\mu\text{M}$), i-mTOR (Rapamycin, $2\mu\text{g/ml}$) i-JNK (SP600125, $20\mu\text{M}$), i-AKT (Akt Inhibitor IV, $0.5\mu\text{M}$), and i-JAK2 (TG-101348, $1\mu\text{M}$), and stimulated \pm FGF (2 ng/ml, 6h). Cyclin D mRNA was measured, the data are fold induction (vs untreated aPFs), the average of > three independent experiments (supports Figure 10).

Supplemental Figure 9

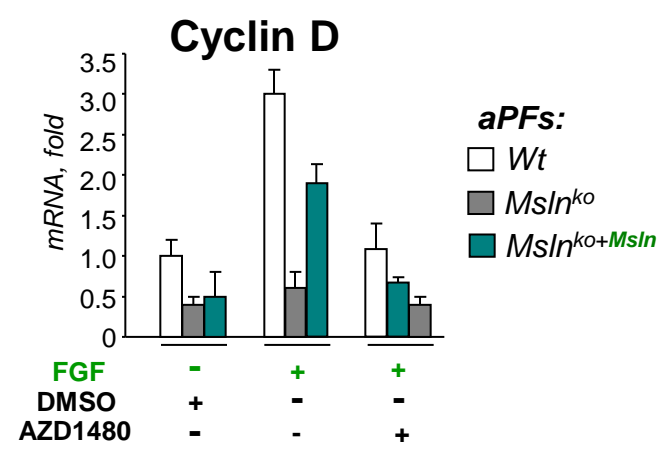
A



B



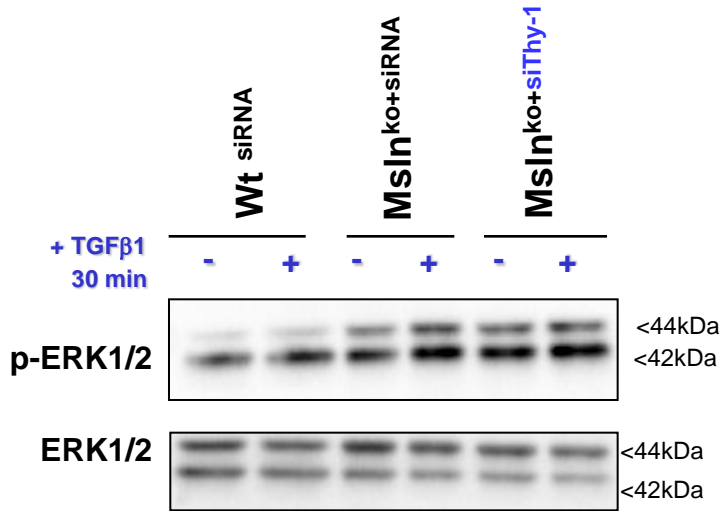
C



Suppl. Figure 9. Reconstitution of Msln in Msln^{ko+Msln} aPFs

A. Msln cDNA was cloned into pCMV-Tag3A expression vector (which also contains *myc* tag at N-terminus, pCMV-Myc) to generate pCMV-Msln-Myc vector. Wt and Msln^{-/-} (Msln^{ko+Msln}) aPFs were transfected either with control vector pCMV-Myc, or pCMV-Msln-Myc. Transfection efficiency was estimated in wt and Msln^{-/-} aPFs by expression of Myc protein using immunostaining with anti-Myc Ab. Similar levels of Myc expression were observed in all transfected cells. Representative images are shown (using objective x 60). **B.** Wt, Msln^{ko+Msln} and Msln^{-/-} aPFs were re-plated after 72 h post transfection (10⁴/well), allowed to adhere overnight (18 h), and analyzed by scratch assay (12 h). The images are bright field (BF) and fluorescent (Col-GFP, taken using objective x 4, average of > three experiments). **C.** Expression of Cyclin D was restored in FGF (2 ng/ml, 6h)-stimulated Msln^{ko+Msln} aPFs and blocked in the presence of AZD1480, P values were determined using ANOVA, * p<0.05, ns - non-specific, (supports Figure 11).

Supplemental Figure 10

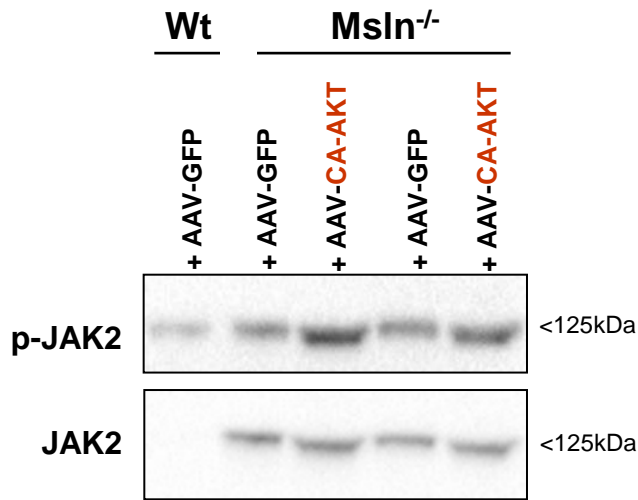


Suppl. Figure 10. Blocking of Thy-1 does not affect expression levels of ERK1/2 in Msln^{ko-siThy-1} aPFs.

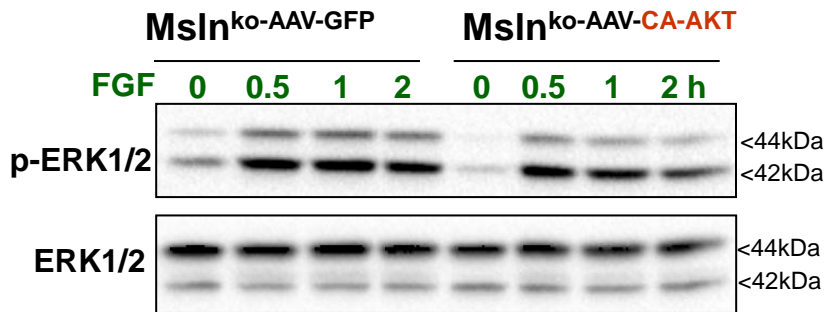
Msln^{-/-} aPFs were transfected with control or Thy-1 (#1, and #4) siRNAs. Expression and phosphorylation of ERK1/2 was evaluated by immunoblotting, normalized to β-actin protein expression level (supports Figure 12).

Supplemental Figure 11

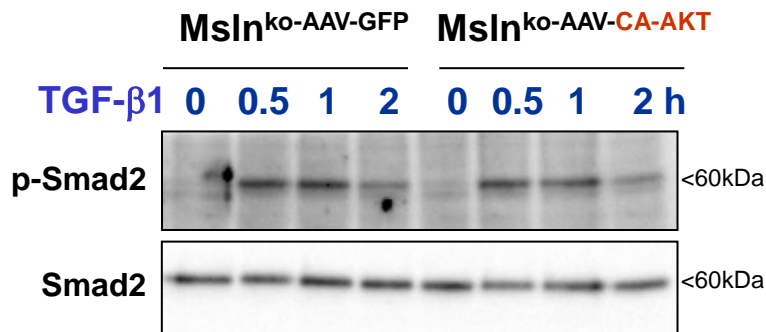
A



B



C



Suppl. Figure 11. Reconstitution of AKT restores proliferation and migration of Msln^{-/-} aPFs.
A. Msln^{-/-} aPFs were infected with constitutively active (CA) AKT (Msln^{ko}-AAV-CA-AKT aPFs). Phosphorylation of JAK2 was restored in Msln^{ko}-AAV-CA-AKT aPFs, normalized to JAK2 protein expression level. **B.** Expression and phosphorylation of ERK1/2 was detected by immunoblotting, normalized to β-actin protein expression level. **C.** TGF-β1-induced phosphorylation of Smad2 was not restored in Msln^{ko}-AAV-CA-AKT aPFs (supports Figure 13).